X-RAY LINE EMISSION FROM EVAPORATING AND CONDENSING ACCRETION DISK ATMOSPHERES

M. A. JIMENEZ-GARATE^{1,3}, J. C. RAYMOND², D. A. LIEDAHL¹, C. J. HAILEY³ Accepted for Part 1 of the Astrophysical Journal

ABSTRACT

We model the X-rays reprocessed by an accretion disk in a fiducial low-mass X-ray binary system with a neutron star primary. An atmosphere, or the intermediate region between the optically thick disk and a Compton-temperature corona, is photoionized by the neutron star continuum. X-ray lines from the recombination of electrons with ions dominate the atmosphere emission and should be observable with the Chandra and XMM-Newton high-resolution spectrometers. The self-consistent disk geometry agrees well with optical observations of these systems, with the atmosphere shielding the companion from the neutron star. At a critical depth range, the disk gas has one thermally unstable and two stable solutions. A clear difference between the model spectra exists between evaporating and condensing disk atmospheres. This difference should be observable in high-inclination X-ray binaries, or whenever the central continuum is blocked by absorbing material and the extended disk emission is not.

Subject headings: accretion, accretion disks — atomic processes — instabilities — line: formation — X-rays: binaries

1. INTRODUCTION

The X-rays reprocessed on accretion disks to the optical, UV and X-ray bands in both X-ray binaries and AGN could be one of our best probes of accretion disk structure and the environment around compact objects. It is convenient to study an illuminated disk around neutron star low-mass X-ray binaries (LMXB) since the central continuum dominates the energetics of the disk atmosphere and accretion disk corona (ADC), and the system geometry is often determined. Measurements of the optical magnitudes and lightcurve amplitudes of LMXB yielded estimates of the angle subtended by the disk of $\sim 12^{\circ}$ and of the average fraction of X-rays reprocessed by the disk into the optical of $\lesssim 0.1$ (de Jong, van Paradijs, & Augusteijn 1996). Models that seem to correctly describe the accretion disk interior have been unable to produce disk geometries consistent with the optical data (Dubus et al. 1999). Analytical models assuming an isothermal disk show better agreement with the data, yet produce illuminated disks that are significantly thinner than expected (Vrtilek et al. 1990).

A pure continuum incident on the gaseous disk will photoionize and heat the gas. Radiative heating sustains a $\sim 10^7 \, \mathrm{K} \, \mathrm{ADC}$ and a smaller $\sim 10^5 \text{--} 10^6 \, \mathrm{K}$ atmosphere emitting X-ray lines on top of the optically thick disk. X-ray spectra of LMXBs during dips show strong Comptonized emission plus an excess flux at 0.65 keV consistent with the same covering fraction (Church et al. 1998), positing that ADC and disks may coexist. The apparent size of the ADC and the disk may not be equal (Church 2000), since the emission mechanisms have different radial dependence. Nayakshin, Kazanas & Kallman (2000) modeled the reprocessed continuum and fluorescence emission from the inner disk of AGN with an ADC, and Ko & Kallman (1994) modeled X-ray spectra of disk annuli in an LMXB with ADC and normally incident radiation.

In this paper, we calculate the structure of an accretion disk illuminated by the grazing radiation of a neutron star in an LMXB with a Compton-temperature ADC, building on a model by Raymond (1993). This model, which we will detail in a future paper, includes a more accurate calculation of the vertical and radial disk structure than previous models, accounts for thermal instabilities, and incorporates recent atomic model calculations that predict X-ray spectra at a resolution superior to the *Chandra* and *XMM*-Newton spectrometers. We obtain the first self-consistent flared disk geometry that matches the disk thickness expected from optical data, and we predict that broad X-ray lines will be observable and will provide, among other diagnostics, evidence for photo-evaporation, which is central to the origin of winds (Woods et al. 1996).

2. Model atmosphere

We consider an LMXB with a $M_* = 1.4 M_{\odot}$ primary radiating an Eddington luminosity bremsstrahlung continuum with T=8 keV. We use a set of fiducial system parameters for a bright LMXB, so application to a particular source will require using the observed X-ray continuum to improve accuracy. The maximum radius of the centrallyilluminated disk is 10^{11} cm, so the orbital period ~ 1 day. The minimum radius is $10^{8.5}$ cm, below which the omitted effect of radiation pressure will dominate.

We obtain the vertical disk atmosphere structure of each annulus by integrating the hydrostatic balance and 1-D radiation transfer equations for a slab geometry:

$$\frac{\partial P}{\partial z} = -\frac{GM_*\rho z}{r^3}$$

$$\frac{\partial F_{\nu}}{\partial z} = -\frac{\kappa_{\nu} F_{\nu}}{\sin \theta}$$
(2)

$$\frac{\partial F_{\nu}}{\partial z} = -\frac{\kappa_{\nu} F_{\nu}}{\sin \theta} \tag{2}$$

Lawrence Livermore National Laboratory, Department of Physics and Advanced Technologies, 7000 East Ave., L-41, Livermore, CA 94550;

² Center for Astrophysics, 60 Garden St., Cambridge, MA 02138; raymond@cfa.harvard.edu

³ Columbia Astrophysics Laboratory, 538 West 120th St., New York, NY 10027; mario@alum.mit.edu, chuckh@astro.columbia.edu

$$\frac{\partial F_{\nu}^{d}}{\partial z} = -\kappa_{\nu} F_{\nu}^{d} \tag{3}$$

while satisfying local thermal equilibrium:

$$\Lambda(P, \rho, F_{\nu}) = 0 \tag{4}$$

where P is the pressure, ρ is the density, F_{ν} is the incident radiation field, F_{ν}^{d} is the reprocessed radiation propagating down towards the disk midplane, z the vertical distance from the midplane, G the gravitational constant, θ the grazing angle of the radiation on the disk, r the radius, and κ_{ν} is the local absorption coefficient. The difference between heating and cooling Λ includes Compton scattering, bremsstrahlung cooling, photoionization heating, collisional line cooling, and recombination line cooling from H, He, C, N, O, Ne, Mg, Si, S, Ar, Ca, and Fe ions. We assume cosmic abundances (Allen 1973). The code from Raymond (1993) computes the net heating and ionization equilibrium, Compton scattering, and line scattering using escape probabilities. A new disk structure calculation simultaneously integrates Eqs. 1-3 by the Runge-Kutta method using an adaptive stepsize control routine with error estimation, and Eq. 4 is solved by a globally convergent Newton's method (Press 1994). At the ADC height z_{cor} , the equilibrium T is close to the Compton temperature $T_{compton}$, from which we begin to integrate downward until $T < T_{phot}(r)$. The optically thick part of the disk, with temperature T_{phot} , is assumed to be vertically isothermal (Vrtilek et al. 1990). To get T_{phot} , we assume that the viscous energy and illumination energy is all locally radiated as blackbody radiation. That is, for $z_{phot} \ll r$ and $R_* \ll r$:

$$\sigma T_{phot}^4 \simeq \frac{3GM_*\dot{M}}{8\pi r^3} + \frac{(1-\eta)L_x \sin\theta(r)}{4\pi r^2}$$
 (5)

where R_* is the neutron star radius, M, L_x the accretion rate and luminosity, σ the Stephan-Boltzmann constant, and $\eta = 0.9$ is the X-ray 'albedo' derived from optical observations (de Jong, van Paradijs, & Augusteijn 1996), such that $1 - \eta$ is the fraction of X-rays absorbed at the photosphere. The height at which the integration ends is defined as the photosphere height z_{phot} . Thus, the assumption is that for $z < z_{phot}$ viscous dissipation dominates heating.

The boundary conditions at the ADC are set to $P(z_{cor}) = \rho_{cor}kT_{compton}/\mu m_p$, $F_x(z_{cor}) = L_x/4\pi r^2$, and $F_{\nu}^d(z_{cor}) = 0$, where $F_x \equiv \int F_v d\nu$, k is the Boltzmann constant, and μ is the average particle mass in units of the proton mass m_p . The boundary conditions at z_{phot} for F_{ν} and F_{ν}^d are set free, and we use the shooting method (Press 1994) with shooting parameter ρ_{cor} adjusted until we satisfy $P(z_{phot}) = \rho_{phot}kT_{phot}/\mu m_p$ at the photosphere. Note ρ_{phot} is the viscosity (α) dependent density calculated for an X-ray illuminated Shakura & Sunyaev (1973) disk.

We calculate $\theta(r)$ iteratively. To get T_{phot} self-consistently from Equation 5, we need $\theta(r) = \arctan(dz_{atm}/dr) - \arctan(z_{atm}/r) + \arctan(R_*/r)$. We neglect the term $\propto R_*/r$, which is valid for $r \gtrsim 10^{8.5}$ cm. After an initial guess for $z_{atm}(r)$, we define it as the height where F_x is attenuated by 1/e. We stop after $\theta(r)$ and T_{phot} converge to $\lesssim 10$ %. Note $F_x \to 0$ for $z \lesssim z_{phot}$. Since z_{atm} is not physically determined, but it is bound by $z_{atm} > z_{phot}$, we ran a second model calculating $\theta(r)$ from z_{phot} , which we will use to estimate systematic errors due to the 1-D radiation transfer calculation.

3. THERMAL INSTABILITY OF THE PHOTOIONIZED GAS

The disk atmosphere exhibits a thermally unstable region, which has direct consequences for the disk structure and X-ray spectrum. The origin of the thermal instability is well understood, and its behaviour depends on metal abundances and the local radiation spectrum (Hess, Kahn, & Paerels 1997).

Within a range of pressure ionization parameters (Ξ), thermal equilibrium is achieved by three distinct temperatures, only two of which are stable to perturbations in T (Fig. 1). $\Xi \equiv 4\pi P_{rad}/P_{gas}$, where $P_{rad} = F_x/4\pi c$ is the radiation pressure and P_{gas} the gas pressure (Krolik, McKee & Tarter 1981). The thermally stable branches have positive slope (Field 1965). Previous spectral studies of illuminated accretion disks in LMXB had not explicitly selected the stable solutions (Ko & Kallman 1994), a choice which affects X-ray production.

The instability implies a large temperature gradient as the gas is forced to move between stable branches, requiring the formation of a transition region whose size may be determined by electron heat conduction, convection, or turbulence, depending on which dominates the heat transfer. For simplicity, we neglect emission from the transition region. Upon calculation of the Field length λ_F , the lengthscale below which conduction dominates thermal equilibrium (Begelman & McKee 1990), we estimate that conduction forms a transition layer $\sim 10^{-2}$ times thinner than the size of the X-ray emitting zones. Nevertheless, X-ray line emission from the neglected conduction region may not be negligible in all cases (Li et al. 2001).

Conduction determines the dynamic behaviour of the gas. The dynamics will allow us to attach a physical interpretation to the chosen solutions from Fig. 1. Roughly, a static conduction solution can only be found if the transition region splits the instability Ξ -range in half (Fig. 1). This solution (Zeldovich & Pikelner 1969) takes the low-T stable branch at $\Xi < \Xi_{stat}$, and the high-T stable branch at $\Xi > \Xi_{stat}$, separated by the transition layer at Ξ_{stat} . A transition layer located away from Ξ_{stat} will dynamically approach Ξ_{stat} by a conduction driven mass flow. A transition layer at $\Xi_{evap} > \Xi_{stat}$ is moving towards lower Ξ , and the gas is evaporating from the low-T branch to the high-T branch. A transition layer at $\Xi_{cond} < \Xi_{stat}$ is moving towards higher Ξ , with the gas condensing to the low-T branch (Zeldovich & Pikelner 1969; Li et al. 2001).

We compute the disk structure for both condensing and evaporating solutions. We assume a steady state, condensing or evaporating mass flow through the transition layer at Ξ_{cond} or Ξ_{evap} , respectively. The static conduction solution is an intermediate case of the latter extreme cases. We take a single-valued $T(\Xi)$, since a two-phase solution would be buoyantly unstable, making the denser (colder) gas sink. The evaporating disk corresponds to the low-T branch, while the condensing disk corresponds to the high-T branch (Fig. 1). This introduces spectral differences (section 6).

We do not know from first principles whether the disk atmosphere is evaporating, condensing, or static. We estimate the speed of the conduction mass flow to be $v_{cond} = 2\kappa T/3P_{gas}\lambda_F$, by using the characteristic conduction time at the Field length, where κ is the Spitzer (1962)

conductivity (for a detailed discussion, see McKee & Begelman 1990). We obtain a conduction mass flow speed v_{cond} which is $1\text{-}2\times10^{-2}$ times the local sound speed. Thus, the phase dynamics will depend on the subsonic ($v\gtrsim v_{cond}$) flow patterns in the disk atmosphere, and these flows will also determine the evaporation or condensation rates.

The only physical mechanism known to transport the necessary angular momentum for disk accretion involves a magneto-rotational instability (MRI) which drives turbulent flow in the disk (Balbus & Hawley 1998). Heat transfer due to this turbulent flow could quench the thermal instability and affect the disk structure. The MRI also favors our assumption of vertical isothermality in the optically thick disk.

4. Spectral modeling

With the disk structure $\rho(r,z)$, T(r,z) and ion abundances $f_{Z,i}(r,z)$, we model the X-ray line emission from the disk atmosphere by using HULLAC (Hebrew University/Lawrence Livermore Atomic Code, Klapisch et al. (1977)). The code calculates the atomic structure and transition rates of radiative recombination (RR) and radiative recombination continuum (RRC) for the H-like and He-like ions of C, N, O, Ne, Mg, Si, S, Ar, Ca, and Fe XVII-Fe XXVI. The emissivities are calculated as described in Sako et al. (1999).

The spectrum for each annulus is added to obtain the disk spectrum. Each annulus consists of a grid of zones in the vertical \hat{z} direction, and T, ρ and $f_{Z,i+1}$ for each zone are used to calculate the RR and RRC emissivities. The radiation is propagated outwards at inclination angle i, including the continuum opacity of all zones above. Compton scattering is not included in the calculated spectrum because it is negligible in the vertical direction in the region where the line emission is formed. The spectrum is Doppler broadened by the projected local Keplerian velocity, assuming azimuthal symmetry.

5. DISK STRUCTURE RESULTS

The self-consistent disk is thicker than would be expected from the local pressure scale height H_P alone. We find $H_P < z_{phot} < z_{atm}$. We fit the modeled photosphere and atmosphere height, z_{phot} and z_{atm} , with Cr^n (r in cm), with fit parameters C and n. We find $C_{phot} = 2.4 \pm 0.4 - 1.9 \times 10^{-3} \ \mathrm{cm}^{1-n_{phot}}, n_{phot} = 1.14 \pm 0.01 + 0.06,$ $C_{atm} = 1.0 \pm 0.1 + 0.2 \times 10^{-3} \ \mathrm{cm}^{1-n_{atm}}, n_{atm} = 1.21 \pm 0.01.$ Thus, $z_{phot} \sim 3$ -4 H_P and $z_{atm} \sim 7$ -8+2 H_P . Estimated systematics are shown, if significant. Vrtilek et al. (1990) estimated $n_{atm} = 9/7 = 1.29$, but in spite of the steeper radial dependence, the Vrtilek disk is thinner, and it equals H_P for $r > 10^{10}$ cm. For comparison to the optically derived disk thickness, z_{atm} is the de facto disk boundary, since a fraction 1/e of the central X-rays have been absorbed there. Thus, previous theoretical studies severely underestimated the disk thickness.

The atmosphere's $(z>z_{phot})$ maximum photoelectric opacity is always $\tau\ll 1$, although $\tau/\sin\theta(r)\gtrsim 1$. Illumination heating dominates at $r\gtrsim 10^{10}$ cm (Eq. 5), where only $F_x(z_{phot})/F_x(z_{cor})\sim 0.12$ of the incident photons reach z_{phot} directly, while $F_x^d(z_{phot})/(F_x(z_{cor})\sin\theta)\sim 0.35$ reach z_{phot} after reprocessing in the atmosphere. Thus, the atmospheric albedo is ~ 0.5 . To reproduce the

disk (atmosphere and photosphere) albedo observed by de Jong, van Paradijs, & Augusteijn (1996) ($\eta \sim 0.9$), the photosphere albedo can be $\lesssim 0.8$, which is a range closer to physical expectations. There is no significant change in the atmosphere structure by varying α from 1 to 0.1.

6. Spectral results

The LMXRB photon flux (photon $\rm cm^{-2}~s^{-1}~keV^{-1})$ is modeled by:

$$F_{\nu}^{tot} = e^{-\sigma_{\nu}N_{H}^{*}}F_{\nu}^{*} + e^{-\sigma_{\nu}N_{H}^{disk}}F_{\nu}^{disk} \tag{6}$$

where F_{ν}^{*} is the neutron star continuum, F_{ν}^{disk} is the RR line and RRC modeled flux, N_{H}^{*} and N_{H}^{disk} are the neutral hydrogen absorption column densities and σ_{ν} are the Morrison & McCammon (1983) absorption cross sections. The system is assumed to be 10 kpc away.

If we let $N_H^* = N_H^{disk}$ in Eq. 6 with i=0, the lines are swamped by the continuum. Thus, low inclination neutron star LMXBs are unlikely to have detectable X-ray lines from the disk. Instead, we consider $N_H^* = 5 \times 10^{22}$ cm⁻² and $N_H^{disk} = 10^{21}$ cm⁻² with $i=75^{\circ}$, where an obscuring medium absorbs half of the continuum flux and is compact enough to leave the disk almost unobscured.

With a partially obscured central continuum, disk evaporation has an observable spectral signature. We simulate 50 ks XMM-Newton RGS 1 and Chandra MEG +1 observations (Fig. 2,3). Some bright lines are shown on Table 1. The evaporating and condensing disks have contrasting O VII/O VIII line ratios. The evaporating disk contains gas at $T \sim 7\text{-}10 \times 10^4$ K, unlike the condensing disk. The H-like ion line intensities are higher for the condensing disk since it has more gas at $T \sim 10^6$ K. The spectral differences stem from the distinct differential emission measure distributions $d(EM)/d\log\Xi$ and from the O VII recombination rate $\alpha_{RR} \propto T^{-\gamma}$, where $\gamma = 0.7\text{-}0.8$, $EM = \int n_i n_e dV$ is the emission measure, and n_i, n_e are the ion and electron densities.

The RRC and He-like line triplet can be used as temperature and density diagnostics, respectively. The RRC width $\propto T$ (Liedahl & Paerels 1996). The forbidden line f of O VII at 22.097 Å is absent due to collisional depopulation at high density, since $\rho\gtrsim 10^{13}~{\rm cm^{-3}}$. The O VII intercombination i to resonance r line ratio is $g=(f+i)/r\simeq i/r\gtrsim 4$, indicating a purely photoionized plasma (Porquet & Dubau 2000). The O VII RRC broadening is Dopplerdominated, resembling the RR lines, while the O VIII RRC has a component with $FWHM\sim 2$ Å that is produced at $T\sim 10^6~{\rm K}$.

7. CONCLUSIONS

Using a model for a disk illuminated by a neutron star, we have produced a global spectrum of X-ray line emission from a self-consistent accretion disk atmosphere. The flaring of the atmosphere matches optical observations (de Jong, van Paradijs, & Augusteijn 1996). For fiducial parameters of a LMXB with a partially obscured central source with Eddington luminosity, observable spectral signatures would identify an evaporating disk atmosphere.

The O VII/O VIII line ratios are a good tracer of evaporation from the disk. The line-rich spectrum has line profiles resolvable by the *XMM* and *Chandra* spectrometers. The lines have broad wings and a double-peaked

core with a velocity from the outermost radius. Only a single line may be resolved since the emission is well distributed throughout $10^{8.5}$ cm $< r < 10^{11}$ cm. He-like triplet diagnostics show signatures of photoionization and high density ($n_e > 10^{13}$ cm⁻³), and H-like RRC are very broad, with a superposed narrow component in evaporating disks.

The distinct spectral signature of evaporation is due to the presence of a thermal instability in the photoionized gas of the disk. This instability cannot be quenched by spectral variations, abundance variations, or optical depth effects (Hess, Kahn, & Paerels 1997). Conduction heating should not affect this result, though turbulent heat transfer or coronal heating might quench the instability if present. In the outer disk, the incident radiative power is $\gtrsim 10$ times the viscous power, so coronal-like heating

should be small.

The X-ray lines from the disk are weak and difficult to detect for a low-inclination LMXB. Only if the inclination is high and a cloudy environment exists do we expect them to be detectable. At press time, an XMM-Newton observation of LMXB dipper EXO 0748-67 has detected broad lines from photoionized gas with $n_e > 7 \times 10^{12} \, {\rm cm}^{-3}$ (Cottam et al. 2001), which we interpret as the disk atmosphere emission, since it confirms the key predictions of our model.

We are grateful to S. Kahn and I. Joseph for fruitful discussions. This work was performed under the auspices of the U.S. Department of Energy by the University of California Lawrence Livermore National Laboratory under contract No. W-7405-Eng-48.

REFERENCES

Allen, C. W. 1973, Astrophysical Quantities (3rd ed.; London: Athlone Press)
Balbus, S. A., & Hawley, J. F. 1998, Rev. Mod. Phys., 70, 1
Begelman, M. C., & McKee, C. 1990, ApJ, 358, 375
Church, M. J. 2000, astro-ph/0012411
Church, M. J., Balucinska-Church, M., Dotani, T., & Asai, K. 1998, ApJ, 504, 516
Cottam, J., Kahn, S. M., Brinkman, A. C., den Herder, J. W., & Erd, C. 2001, A&A, 365, L277
de Jong, J. A., van Paradijs, J., & Augusteijn, T. 1996, A&A, 314, 484
Dubus, G., Lasota, J. P., Hameury, J. M., & Charles, P. 1999, MNRAS, 303, 139
Field, G. B. 1965, ApJ, 142, 531
Hess, C. J., Kahn, S. M., & Paerels, F. B. S. 1997, ApJ, 478, 94
Klapisch, M., Schwab, J. L., Fraenkel, J. S., & Oreg, J. 1977, Opt. Soc. Am., 61, 148
Ko, Y., & Kallman, T. R. 1994, ApJ, 431, 273
Krolik, J. H., McKee, C. F., & Tarter, C. B. 1981, ApJ, 249, 422
Li, Y., Gu, M. F., & Kahn, S. M., submitted to ApJ

Morrison, R., & McCammon, D. 1983, ApJ, 270, 119
Liedahl D. A., & Paerels F. 1996, ApJ, 468, 33
McKee, C. F. & Begelman, M. C. 1990, ApJ, 358, 392
Nayakshin, S., Kazanas, D., & Kallman, T. R. 2000, ApJ, 537, 833
Porquet, D., & Dubau, J. 2000, A&A, 143, 495
Press, W. H. 1994, Numerical Recipes in FORTRAN: The Art of Scientific Computing (Cambridge: Cambridge University Press)
Raymond, J. C. 1993, ApJ, 412, 267
Sako M., Liedahl, D. A., Kahn, S. M., & Paerels, F. 1999, ApJ, 525, 921
Shakura, N. I., & Sunyaev, R. A. 1973, A&A, 24, 337
Spitzer, L. 1962, Physics of Fully Ionized Gases, (New York: Interscience)
Vrtilek, S. D., Raymond, J. C., Garcia, M. R., Verbunt, F., Hasinger, G., & Kurster, M. 1990, A&A, 235, 162
Woods, D. T., Klein, R. I., Castor, J. I., McKee, C. F., & Bell, J. B. 1996, ApJ, 461, 767
Zeldovich, Y. B., & Pikelner, S. B. 1969, Soviet Physics JETP, 29,

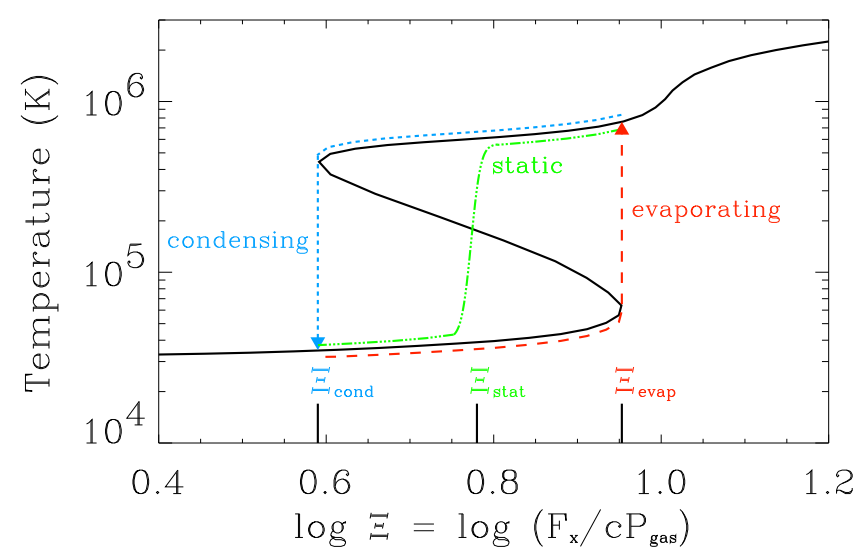


Fig. 1.— Ionization parameter Ξ vs. temperature assuming an 8 keV bremsstrahlung continuum. The s-curve corresponds to the locus of solutions in thermal balance and ionization equilibrium. We model the extreme cases, the evaporating and condensing disks, which correspond to the lower and upper stable branches of the curve, respectively. The inclusion of conduction in the energy equation modifies the thermal equilibrium locus, creating solutions with one small transition region. Schematics of the static transition region at Ξ_{stat} and two dynamic transition regions at Ξ_{cond} and Ξ_{evap} are shown. For $\log \Xi > 1.2$, T increases up to $T_{compton} \sim 10^7$ K (not shown).

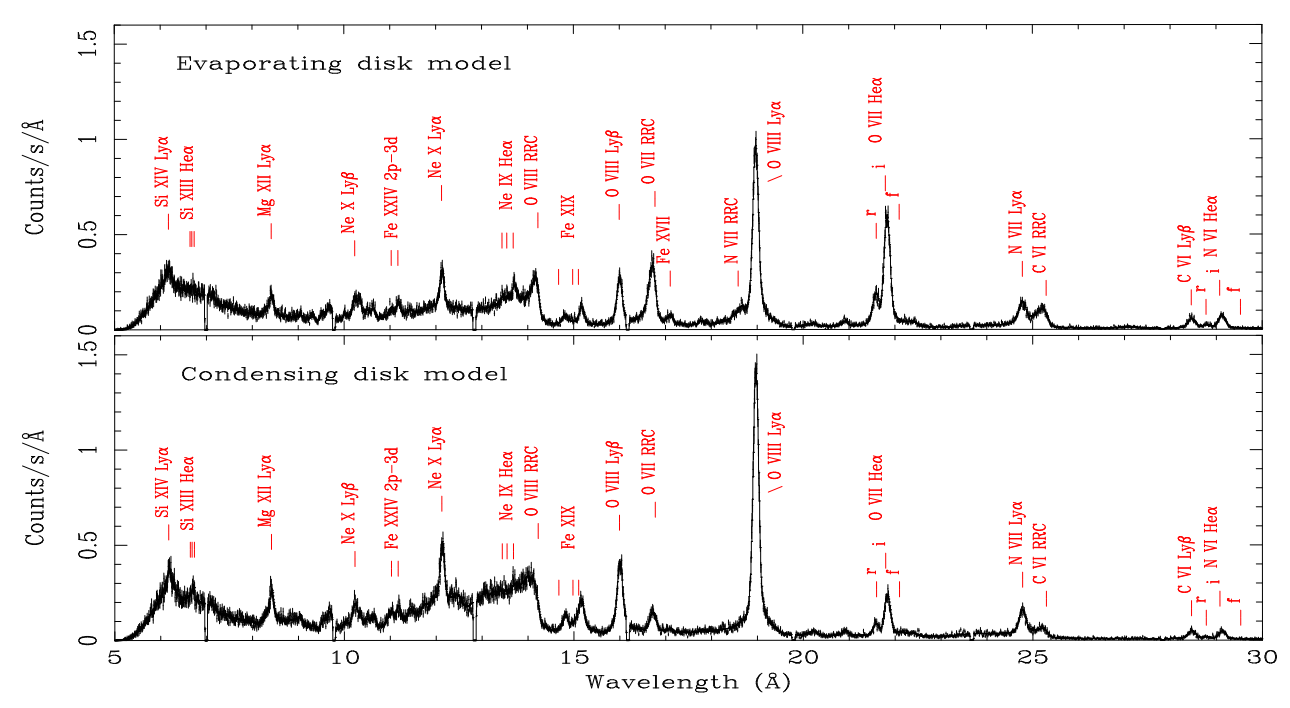


Fig. 2.— Spectra for evaporating and condensing accretion disks. Simulated 50 ks observation with XMM-Newton RGS 1. The continuum emission from the inner ($r < 10^{8.5}$ cm) disk is not included, and the obscuration of the ionizing continuum from the compact object is assumed.

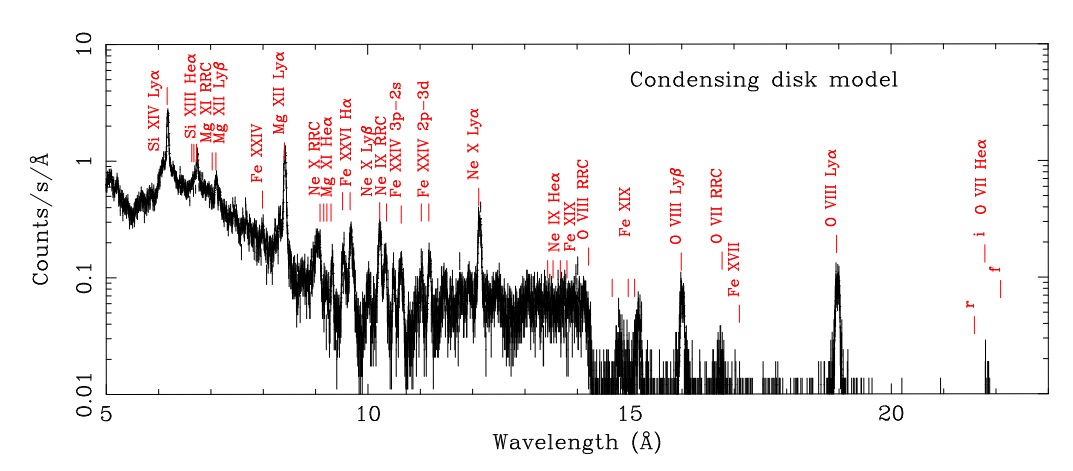


Fig. 3.— Condensing disk spectrum (as in Fig. 2). Simulated 50 ks observation with Chandra MEG 1.

 $\label{eq:table 1} \text{Line fluxes for two disk models.}$

| Line(s) | Evaporating ^a | Condensinga |
|---|--------------------------|-------------|
| O VII He α triplet | 2.1 | 0.99 |
| O VIII Ly α | 3.4 | 4.7 |
| O VII RŘC | 1.3 | 0.61 |
| O VIII Ly β | 0.94 | 1.5 |
| Fe XIX L (0.815 keV) | 0.45 | 0.91 |
| Ne \hat{X} Ly α | 1.4 | 2.2 |
| Fe XXVI H α (1.28 keV) | 0.74 | 0.86 |
| $Mg XII Ly\alpha$ | 1.2 | 2.0 |
| Si XIII He α triplet | 1.2 | 2.4 |
| Si XIV Ly α | 4.0 | 6.0 |
| Fe XXV $Ly\alpha$ | 15 | 16 |
| Fe XXVI $\overset{\circ}{\mathrm{Ly}} \alpha$ | 12 | 12 |

 $^{^{\}rm a}{\rm Line}$ fluxes in units of $10^{-12}~{\rm erg~cm^{-2}~s^{-1}}$, typically over an interval $E/\Delta E\sim 100.$ Estimated systematic normalization error limit of ~ 50 %, due to the 1-D calculation.